



ELSEVIER

Solid State Ionics 96 (1997) 153–172

**SOLID  
STATE  
IONICS**

## Experimental limitations in impedance spectroscopy: Part III. Effect of reference electrode geometry/position

G. Hsieh<sup>a</sup>, T.O. Mason<sup>a,\*</sup>, E.J. Garboczi<sup>b</sup>, L.R. Pederson<sup>c</sup>

<sup>a</sup>Department of Materials Science and Engineering, Northwestern University, Evanston, IL 60208, USA

<sup>b</sup>National Institute of Standards and Technology, Building Materials Division, Gaithersburg, MD 20899, USA

<sup>c</sup>Materials and Chemical Sciences Department, Pacific Northwest Laboratory, Richland, WA 99352, USA

Received 26 June 1996; accepted 10 January 1997

---

### Abstract

Experiments and computer simulations on Pt/YSZ specimens in various electrode configurations were performed to investigate the effect of reference electrode geometry/position on the accuracy of impedance measurements. The internal, Luggin probe-type, geometry is the preferred reference electrode configuration as it accurately measures both electrolyte and electrode impedances. External, 'pseudoreference', electrodes sample an averaged effective potential and can register inaccurate electrolyte resistances, sometimes with distorted electrode arcs. A symmetric configuration can accurately measure the impedance of an electrode; however, the electrolyte resistance will not scale linearly according to sample dimensions, as one might expect. An asymmetric configuration exhibits both non-linear partitioning of electrolyte resistance and distortions in the electrode impedance arc under certain circumstances. The reliability of three-electrode measurements is very sensitive to aspect ratio and electrode configuration.

*Keywords:* Impedance spectroscopy; YSZ; Pt electrode; Ag electrode; Reference electrode

---

### 1. Introduction

In spite of the extensive use of reference electrodes in electrochemical studies, detailed investigations of the role of reference electrode geometry/placement in impedance measurements are lacking. This is especially the case for solid electrolyte/electrode systems, where geometrical limitations can severely constrain possible electrode configurations. In Parts I [1] and II [2] of this series, we addressed the influence of large reference electrode impedance

on three-point impedance measurements. The present work investigates the influence of electrode geometry/placement, especially the reference electrode, on three-point DC-resistance and AC-impedance measurements.

A number of prior studies have addressed problems associated with reference electrode position/orientation in DC electrochemical cells. Kasper [3] considered the problem of potential distribution versus electrode orientation in simple cells. Barnartt [4] carried out extensive mapping of equipotential surfaces versus electrode size/shape. By similar mapping, Pizzini et al. [5] revealed that discontinuities and abrupt changes in cell geometry cause

---

\*Corresponding author. Tel.: +1 847 491 3198; fax: +1 847 491 7820; e-mail: t-mason@nwu.edu

nonuniform, high local current densities, resulting in closely spaced equipotential surfaces with high curvature. The potential of a finite size reference electrode placed near these locations is ambiguous because it samples many equipotential surfaces. Since primary current becomes nonuniform at the edge of an electrode, termination of an electrode also causes nonuniform ohmic potential drops [6,7]. Calculations showed that serious errors can result in measurements of electrode kinetic parameters. The magnitude of the error depends on the position of the reference electrode with respect to the working electrode and can reach as high as 300 percent. In determination of exchange current density,  $i_0$ , for systems obeying Tafel kinetics, a reference electrode situated at infinity with respect to a disk-shaped working electrode is less susceptible to such errors than a reference situated at the center or the edge of the disk. Nagata et al. [8] showed a similar position dependence with overpotential measurements. Measurements on yttria stabilized zirconia (YSZ) with external platinum reference electrodes showed that apparent overpotential varied with reference electrode position. DC circuit analysis confirmed that overpotential can be measured accurately only when the reference electrode is placed far from both the working and the counter electrode. Electrode configurations with high aspect ratios (i.e. with separation between the reference electrode and the working electrode at least thirty times the thickness of the electrolyte) were suggested by van Heuveln et al. [9].

Immersion of a Luggin capillary reference electrode into the electrolyte between parallel plate working and counter electrodes is another method to accurately measure electrode overpotential [10,11]. An additional advantage of this geometry is that by bringing the tip of the Luggin probe close to the working electrode, the contribution from the electrolyte resistance can be reduced. In order to avoid perturbing the equipotential surfaces near the working electrode as a result of the close proximity of the reference electrode, Barnartt [10] suggested that for a Luggin capillary with radius  $r$ , the separation between the tip of the capillary to the working electrode should be no less than  $4r$ .

With any cell geometry and electrode position, it is necessary to quantify and subtract the electrolyte contribution from the measured potential, especially when the reference electrode is far from the working

electrode. Impedance spectroscopy is a favored technique for this purpose, as it can clearly separate the electrode response from the electrolyte resistance. While it is known that the position of the reference electrode can influence DC measurements, little has been reported concerning the effect of reference electrode geometry/placement on impedance spectra. Fiaud et al. [12] reported that electrochemical impedance is strongly dependent on reference electrode position. Both the apparent electrolyte resistance and the shape of the electrode arc change with reference electrode placement. Despite this fact, many cell geometries are currently used in impedance studies, especially in solid electrolyte systems, even though the effects of reference electrode geometry/placement on the accuracy of the measurement have not been fully characterized. Arrangements similar to configurations 1 and 2 in Fig. 1 are

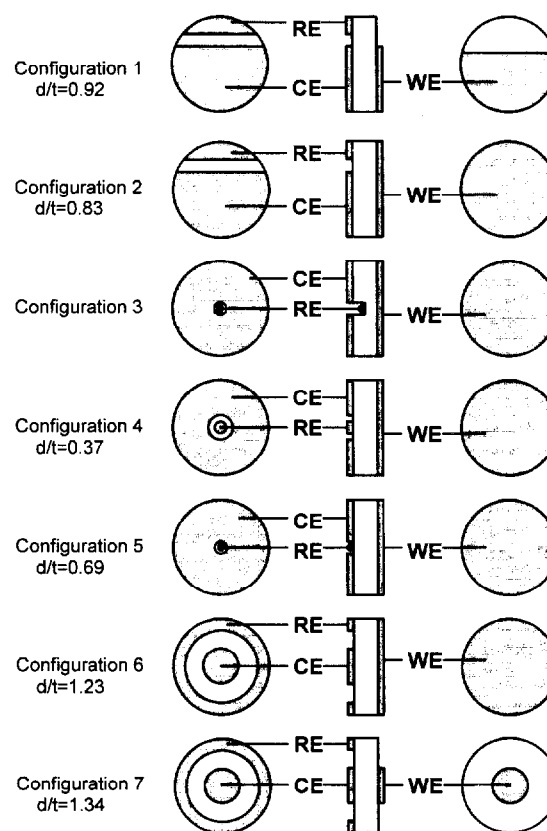


Fig. 1. Various configurations of electrode placement on YSZ. Configuration 3 is the solid electrolyte analog of the Luggin capillary reference used in aqueous systems.

frequently encountered [13–18]. The radially symmetric configurations 6 and 7 are also common [10,19,20]. Generally, surface-mounted pseudoreference electrodes can be divided into two categories: symmetric configurations, where the counter and working electrodes are of the same size and shape opposite each other, and asymmetric configurations, where the electrodes are not of the same shape or size. Recently, solid state analogs of the Luggin probe and embedded reference electrode for thin-film work have been developed [21,22].

The present work addresses the effects of reference electrode placement on the accuracy of impedance measurements. A variety of commonly encountered configurations was tested using zirconia solid electrolyte and porous platinum electrodes. To better understand the origin of errors, certain configurations were also examined by computer simulations. The limitations of surface-mounted reference electrodes, hereafter referred to as ‘pseudoreference’ electrodes, and the reliability of a Luggin probe-type reference electrode geometry are discussed, in the context of solid electrolyte/electrode systems.

## 2. Experimental

Yttria stabilized zirconia (YSZ) powder with 8 mole %  $Y_2O_3$  (Tosoh Corp., Japan) was isostatically pressed into disks without a binder. Samples were sintered to ~99% theoretical density at 1400°C in air

for 2 h. The diameters of the sintered samples were ~1.70 cm, and the thicknesses were ~0.25 cm. After diamond-polishing the flat ends to 1  $\mu\text{m}$  finish, unfluxed platinum paint (Engelhard Corp., Newark, NJ) was applied to the surfaces to form the working electrode (WE), the counter electrode (CE) and the pseudoreference electrode (RE). The paint was dried at 300°C and then fired at 900°C for 20 min. Two coats of platinum paint were applied to form each electrode. Platinum wire mesh served as current collectors. Fig. 1 shows the geometries of the WE and CE, the position of the RE, and the corresponding aspect ratios. To characterize the pseudoreference electrode configurations, we define the ‘aspect ratio’ as the separation between the RE and CE ( $d$ ) divided by the sample thickness ( $t$ ). Configuration 3 is an adaptation of the Luggin probe-type reference electrode. A small axial hole (~1 mm diameter) was drilled into the electrolyte using an ultrasonic diamond drill to the depth desired. The reference electrode was a 0.010" diameter silver wire with one end melted into a small bead. The wire was inserted into a 0.80 mm OD alumina thermocouple protection tube and the bead was pulled tight against the end of this tube. The tube was then inserted into the hole in the YSZ and mechanically pressed against the YSZ by a spring-loaded fixture. The same point-reference electrode was used in configuration 5, but it was not embedded within the electrolyte.

Additional cells were constructed with two reference electrodes, an embedded silver reference and a

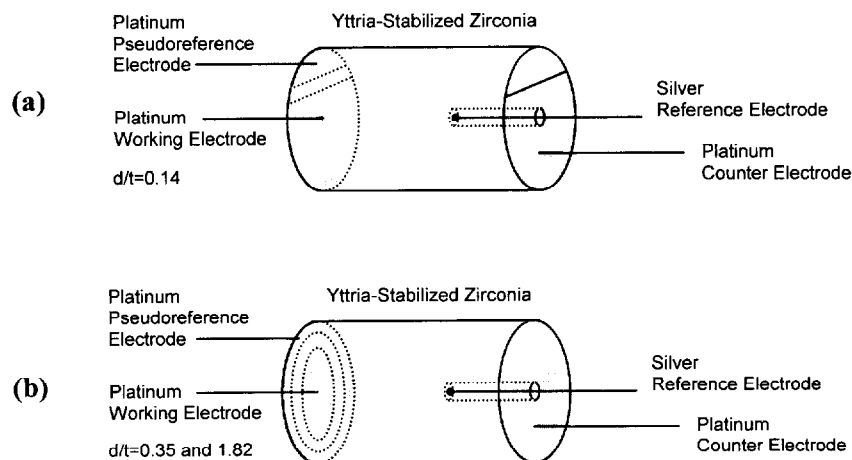


Fig. 2. Pt/YSZ/Pt cells with both platinum pseudoreference and embedded silver reference: (a) configuration 1 and 3 combined; (b) configuration 6 and 3 combined.

platinum pseudoreference, as in Fig. 2. The diameter of the electrolyte disk was 1.68 cm while the thickness was increased to 0.83 cm. The depth of the axial hole was approximately 1/4 of the disk thickness. This dual-reference design allowed characterization of an identical electrode/electrolyte system by two difference reference electrodes. Other details were as previously described.

The Pt/YSZ/Pt cells were heated in a tube furnace and measurements were made in air at 700°C. Impedance scans were collected in two-point and three-point configurations in order to obtain combined and individual impedances of the working and the counter electrode, along with contributions from the electrolyte. The Solartron 1260 frequency response analyzer (1260 FRA) was employed without a potentiostat in the differential voltage sensing mode. The frequency range was from 1 MHz to 10 mHz. In three-point measurements, the effects of reference electrode impedance were taken into consideration [1,2]. Both HI-pin and LO-pin three-point spectra were measured (see [1] for an explanation). For cases where the reference electrode impedance was high, a correction routine was used to obtain the 'true' impedance [2]. Analysis of impedance spectra by equivalent circuit fitting was carried out using Boukamp's EQUIVCRT program [23].

Computer simulations of impedance spectra were performed using a 3-D pixel-based model [24–27]. For this work the size of the model was  $90 \times 90 \times 12$  pixels, corresponding to approximately  $0.2 \text{ mm}^3$  per pixel volume. The complex Laplace's equation is discretized using either a finite difference method [27], where a node is placed in the center of each pixel, or a finite element method, where each pixel is treated as a tri-linear finite element [28], with nodes on the pixel corners. The linear equations that result are solved using a conjugate gradient relaxation method [28,29]. First, DC simulations were done to investigate the effect of reference electrode position on the partitioning of electrolyte resistance. This was accomplished by letting the WE and CE impedances be zero. Next, AC simulations were performed for configurations 1, 3 and 6 (Fig. 1) to observe the effects of reference electrode position on measurement of electrode impedances. For these simulations, the WE and CE impedance arcs are represented as two depressed semicircles. Each is described by a

Table 1

Values used in numerical simulation of electrode impedance. As input, the working and counter electrode impedances are simulated as two depressed semicircles (RQ), using EQUIVCRT notation [23]

	$R$	$Q_0$	$n$
Working electrode	150 $\Omega$	$2.5 \times 10^{-5}$ F	0.850
Counter electrode	250 $\Omega$	$1.5 \times 10^{-5}$ F	0.700
YSZ conductivity = $0.0185 \text{ S cm}^{-1}$			

network of resistor and constant phase element (CPE) in parallel, or (RQ) in the EQUIVCRT notation [23]. The parameters for the simulations are listed in Table 1. They were chosen to reflect typical values observed. In addition, simulations of the dual reference electrode systems in Fig. 2 were also performed.

### 3. Results and discussions

Table 2 shows the partitioning of electrolyte resistance for cell configurations 1 through 7, as measured on Pt/YSZ/Pt specimens by impedance spectroscopy. For configuration 3, the Luggin probe hole extended 1/3 of the specimen thickness. Columns denoted RE/CE and RE/WE are electrolyte resistances observed in the CE and WE spectra, respectively. Electrolyte resistance is the high frequency intercept in the Nyquist plot. The values listed in Table 2 are normalized by the total electrolyte resistance between the working and counter electrodes.

Table 2

Partitioning of electrolyte resistance between RE and CE and between RE and WE. Values are normalized by the total electrolyte resistance between CE and WE in each configuration. Experimental measurements and computer simulation are shown

Configuration	Measured		Simulation	
	RE/CE	RE/WE	RE/CE	RE/WE
1	0.504	0.496	0.490	0.510
2	0.842	0.158	0.900	0.100
3	0.378	0.622	0.350	0.650
4	0.505	0.495	0.440	0.560
5	0.501	0.499	0.498	0.502
6	0.920	0.080	0.946	0.054
7	0.373	0.627	0.390	0.610

The fractions of electrolyte resistance observed are indications of the location of the effective equipotential surface sampled by the reference electrode in each electrode configuration. In configuration 3, the current density is expected to be uniform as perturbation due to the presence of the reference electrode is small. Consequently, the equipotential surfaces are planar and parallel to the working and counter electrodes. The actual surface sampled by the reference electrode is the surface tangent to the tip of the reference electrode, and the potential is well defined. As expected, the partitioning of electrolyte resistance (potential) scales with RE position relative to the two electrodes ( $\sim 1/3$  versus  $\sim 2/3$  of overall CE/WE separation). In contrast, the effective potentials of the pseudoreference electrodes in the remaining configurations are not well defined. One could naively assume that the RE/CE resistance (potential) should be approximately zero if these two electrodes are on the same face of the sample, especially if they are in close proximity. Instead, the RE is found to be at an intermediate potential which can be a substantial fraction of the overall WE/CE potential, as if the RE were located in the interior of the specimen. (In configuration 6, for example, the partitioning is as if the RE were close to the WE rather than the CE.) The reason for this behavior is that, except for configuration 3, the RE is located in regions of nonuniform current density. Furthermore, except for configurations 3 and 5, all reference electrodes have relatively large areas and therefore sample a range of equipotential surfaces. Consequently, an average potential is obtained. The interpretation of the electrolyte resistance is not straightforward as there is no simple relationship between resistance and geometry. Van Heuveln et al. [9] similarly found that the relative position of pseudoreference electrodes does not coincide with the physical electrode spacing. This ambiguity is complicated by the fact that the pseudoreference electrode in the present study is not located at infinity relative to the WE and CE. Whereas van Heuveln et al. used configurations with high aspect ratios (RE/WE and RE/CE spacings  $\sim 30$  times sample thickness), the present experiments used much smaller electrode spacings.

To confirm experimental observations, computer simulations of DC resistances were performed. The results are also shown in Table 2. There is good

agreement between simulation and experiment. The small differences can be attributed largely to the use of a model with discrete nodes to approximate a distributed physical system and the difficulty in exactly reproducing the experimental configurations in the simulation input. The good agreement confirms that the experimental observations are not artificial and validates the computer model as an alternate method to investigate the effects of reference electrode position.

Simulations also permit investigation of impedance measurements of electrode responses. Unlike actual experiments, for which the true electrode response is an unknown, we can assign a representative response (i.e., assigned equivalent circuit parameters) and test whether or not a given reference electrode geometry accurately measures that response.  $Z'-Z''$  plots of complete AC simulations on electrode configurations 1, 3 and 6 are plotted in Figs. 3, 5 and 6, respectively. For configurations 1 and 6, results for several different aspect ratios are shown. These configurations were chosen because they are typical of the symmetric and asymmetric arrangements commonly encountered in literature. Both the apparent CE and WE spectra, as 'measured' at the RE by three-point method, are shown. The 'actual' impedance spectra are computed from the known input parameters listed in Table 1, with the high frequency intercept adjusted (to compensate for the DC problems discussed previously) to match that of the apparent spectra in order to make any deviations in the electrode arc readily discernable.

As shown in Fig. 3, there is no noticeable difference between the apparent and the actual impedance responses of the CE or the WE in configuration 1. The magnitude of the impedance arcs is correct although the electrolyte resistance is subject to the peculiar partitioning previously discussed. Over a range of aspect ratios  $d/t$ , there is no appreciable error in the size of the apparent impedance arc from the true values (see Fig. 4a). Note that the  $x$ -axis is inverse aspect ratio, which can be loosely interpreted as sample length. In Fig. 4b, the sum of electrolyte resistances scales linearly with inverse aspect ratio, a somewhat surprising result considering the ill-defined nature of the sampling potential. The linear trend, however, does not pass through the origin. Broken down into the individual WE and CE com-

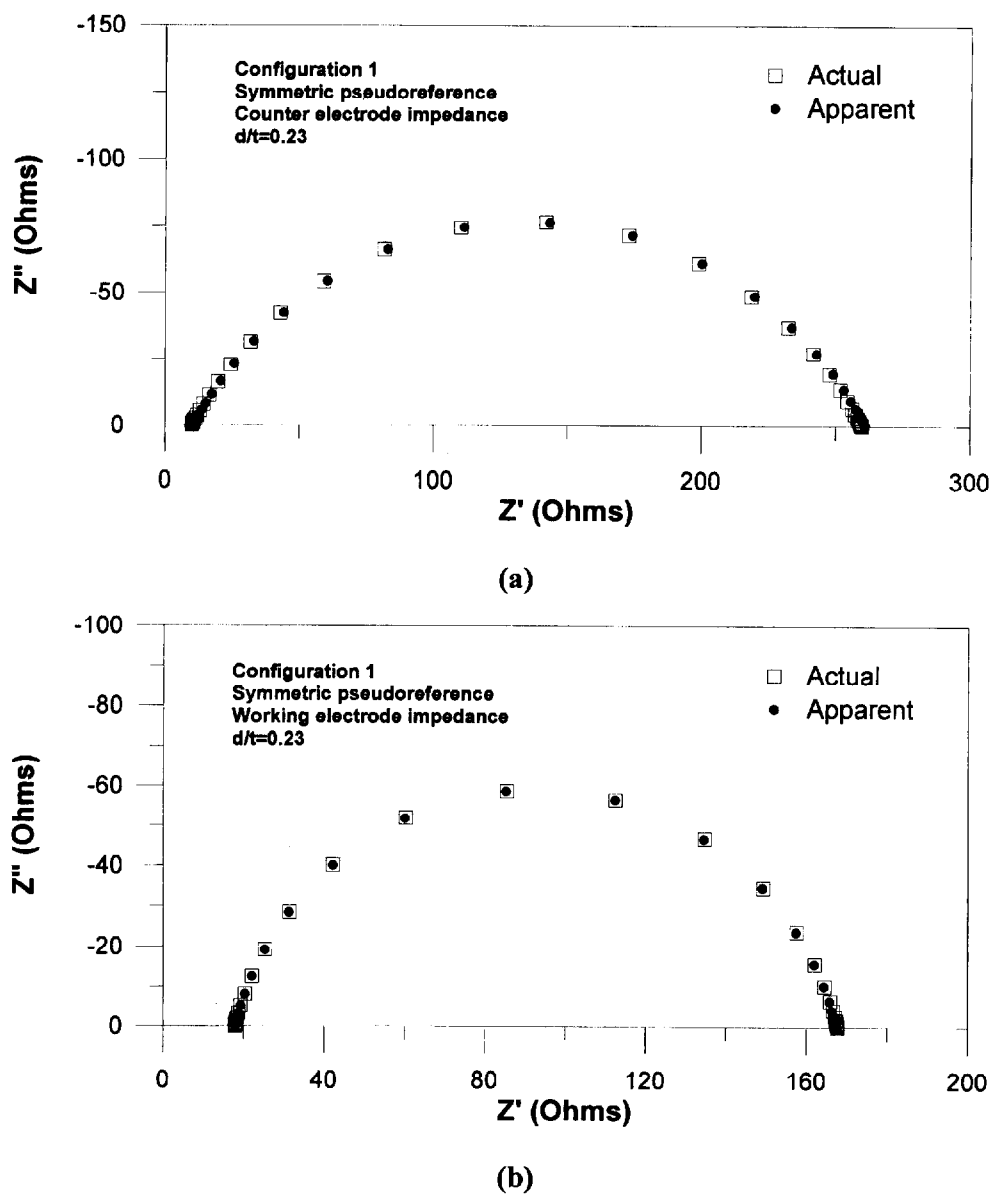
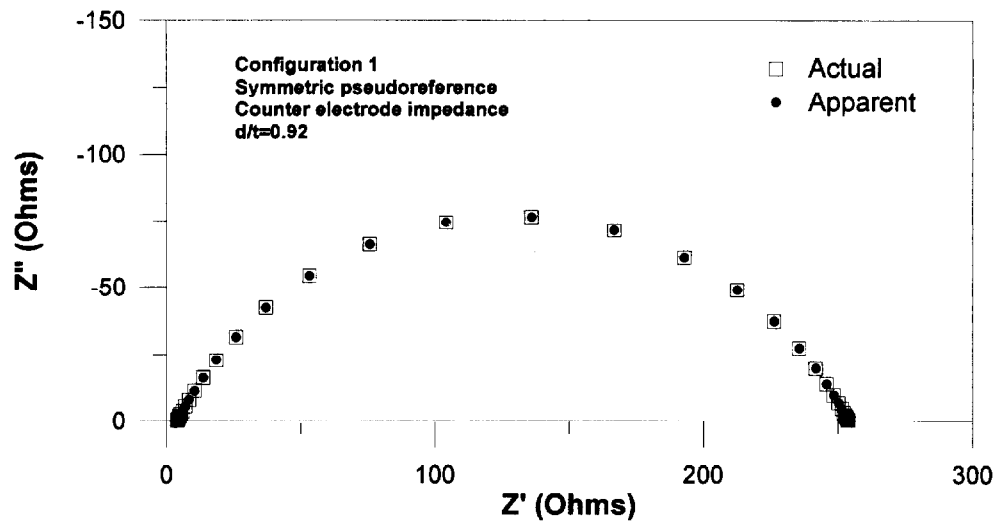


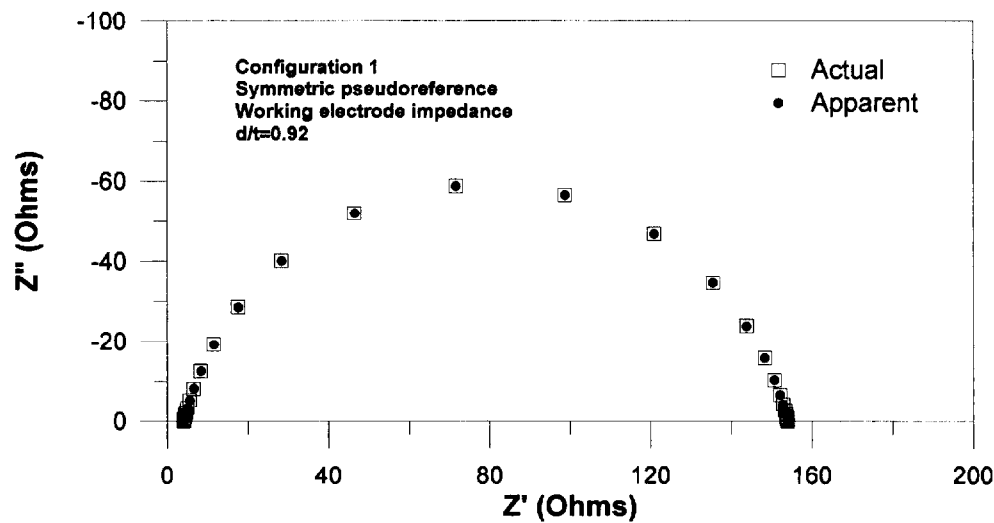
Fig. 3. Simulated actual (□) and apparent (●) impedance spectra using electrode configuration 1, the symmetric pseudoreference electrode: (a) counter electrode,  $d/t = 0.23$ ; (b) working electrode,  $d/t = 0.23$ ; (c) counter electrode,  $d/t = 0.92$ ; (d) working electrode,  $d/t = 0.92$ ; (e) counter electrode,  $d/t = 3.68$ ; (f) working electrode,  $d/t = 3.68$ .

ponents in Fig. 4c, total electrolyte resistance is divided evenly between the WE and the CE when reference electrode separation ( $d$ ) is comparable or larger than electrolyte thickness ( $t$ ). As thickness increases with respect to electrode separation, the partitioning becomes increasingly uneven, and the

effective potential surface sampled by the pseudoreference electrode moves from the middle toward the counter electrode. Consistent with the findings of Nagata et al. [8] and van Heuveln et al. [9] these results suggest that in situations where tape-cast or other thin-film electrolytes are used, it is possible to



(c)



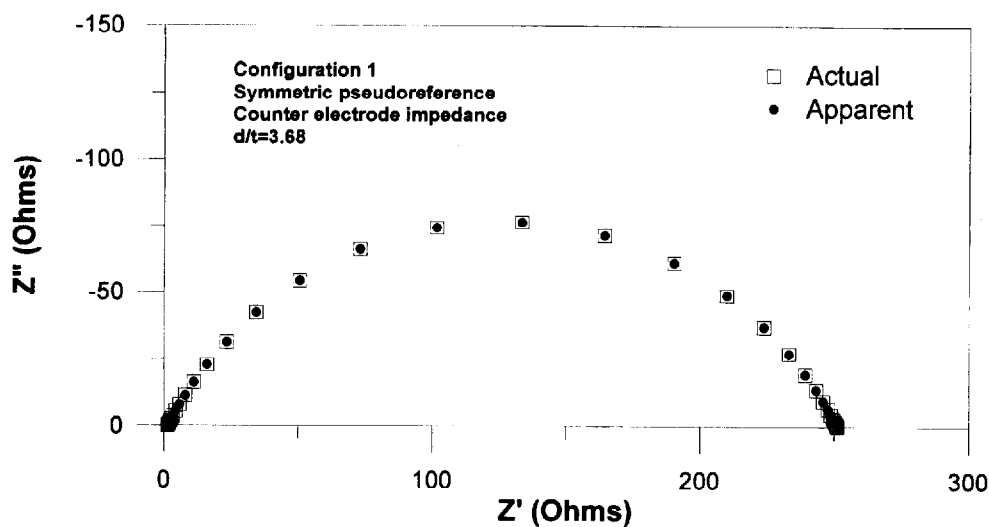
(d)

Fig. 3. (continued)

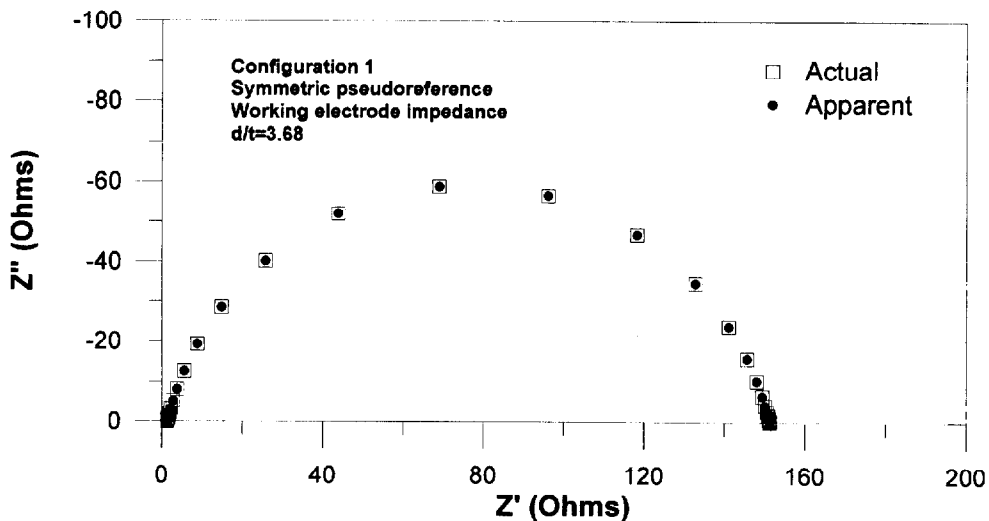
treat a surface pseudoreference electrode mounted far from either counter or working electrode, in a symmetric configuration, as if it is actually located in the middle of the electrolyte without significant loss of accuracy.

Fig. 5 shows simulated impedance spectra for an embedded Luggin-probe type reference electrode.

The apparent impedance is the true impedance. Although only one simulation was performed, it is expected that changing the depth of the probe will not affect accuracy provided the separation from the tip of the probe to the WE and CE is much larger than the radius of the probe [10]. Because the sampled potential is well defined, the partitioning of



(e)



(f)

Fig. 3. (continued)

electrolyte resistance scales linearly with the depth of the probe. For studies where the electrolyte is thick, this is the preferred electrode configuration as very large samples are required to achieve sufficiently large  $d/t$  in the symmetric electrode configuration. One should be aware, however, that a point probe may result in large reference electrode impedances

which can cause distortions from the voltage divider effect [1,2].

In contrast, apparent impedances simulated using configuration 6, shown in Fig. 6, exhibit gross distortions. The distorted spectra show large phase shifts, inaccurate electrode resistances, and artificial features. In particular, the CE spectra show a second

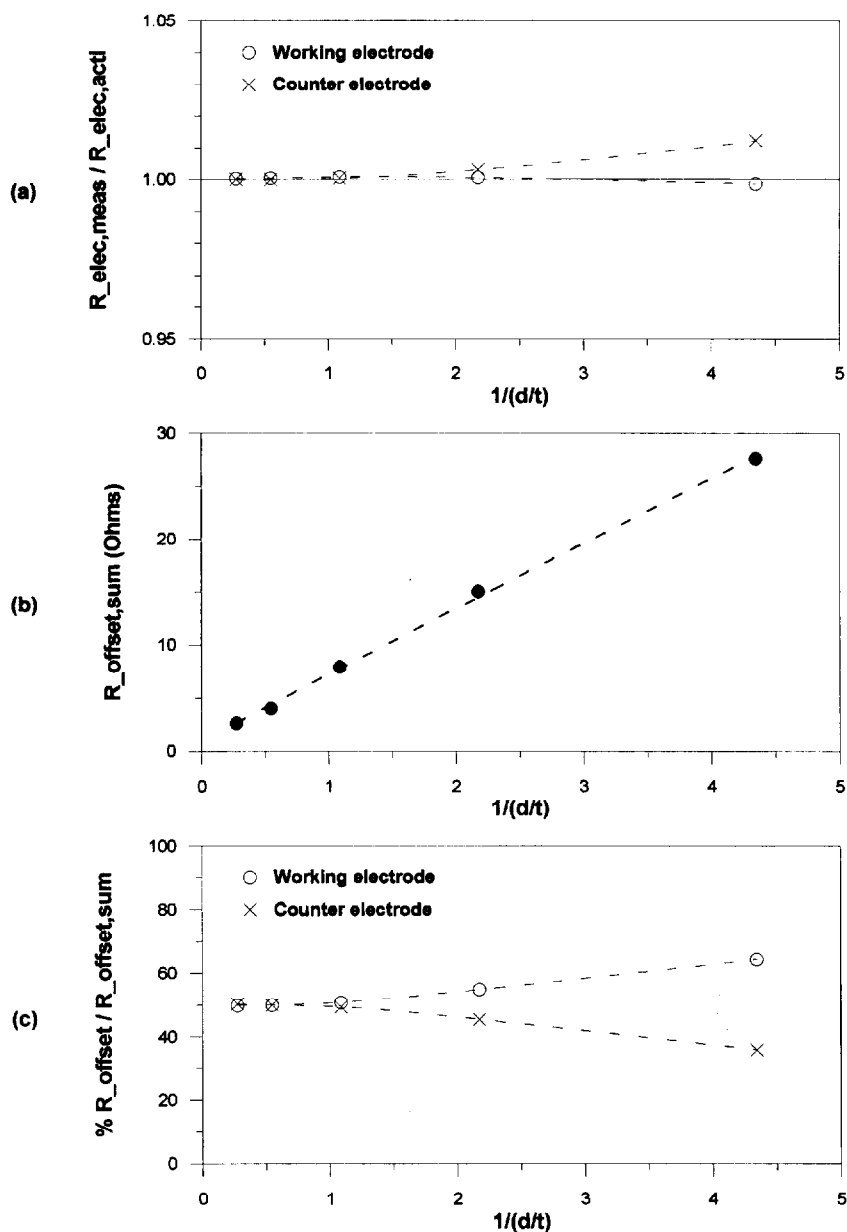


Fig. 4. Effect of aspect ratio  $d/t$  on the accuracy of symmetric electrode configuration 1: (a) deviation of apparent magnitude of working electrode ( $\circ$ ) and counter electrode ( $\times$ ) arc from input parameters where  $R_{elec,meas}$  is the measured electrode resistance and  $R_{elec,act}$  is the actual electrode resistance; (b) total electrolyte resistance  $R_{offset,sum}$  is the sum of high frequency offsets from the working electrode and counter electrode spectra; (c) individual partitioning of electrolyte resistance, expressed as fraction of total electrolyte resistance.

high frequency arc, and the WE spectra exhibit phase shifts into the  $-Z'$  quadrant. Both of these distortions are artifacts. The magnitude of the distortion appears to be minimal as  $d/t$  is reduced below 0.50

(or  $(d/t)^{-1} > 2$  in Fig. 7a). Thus, for such asymmetric electrode arrangements, data may be reliable at some aspect ratios but not at others, and it is desirable to have small ratios (thick samples). Not

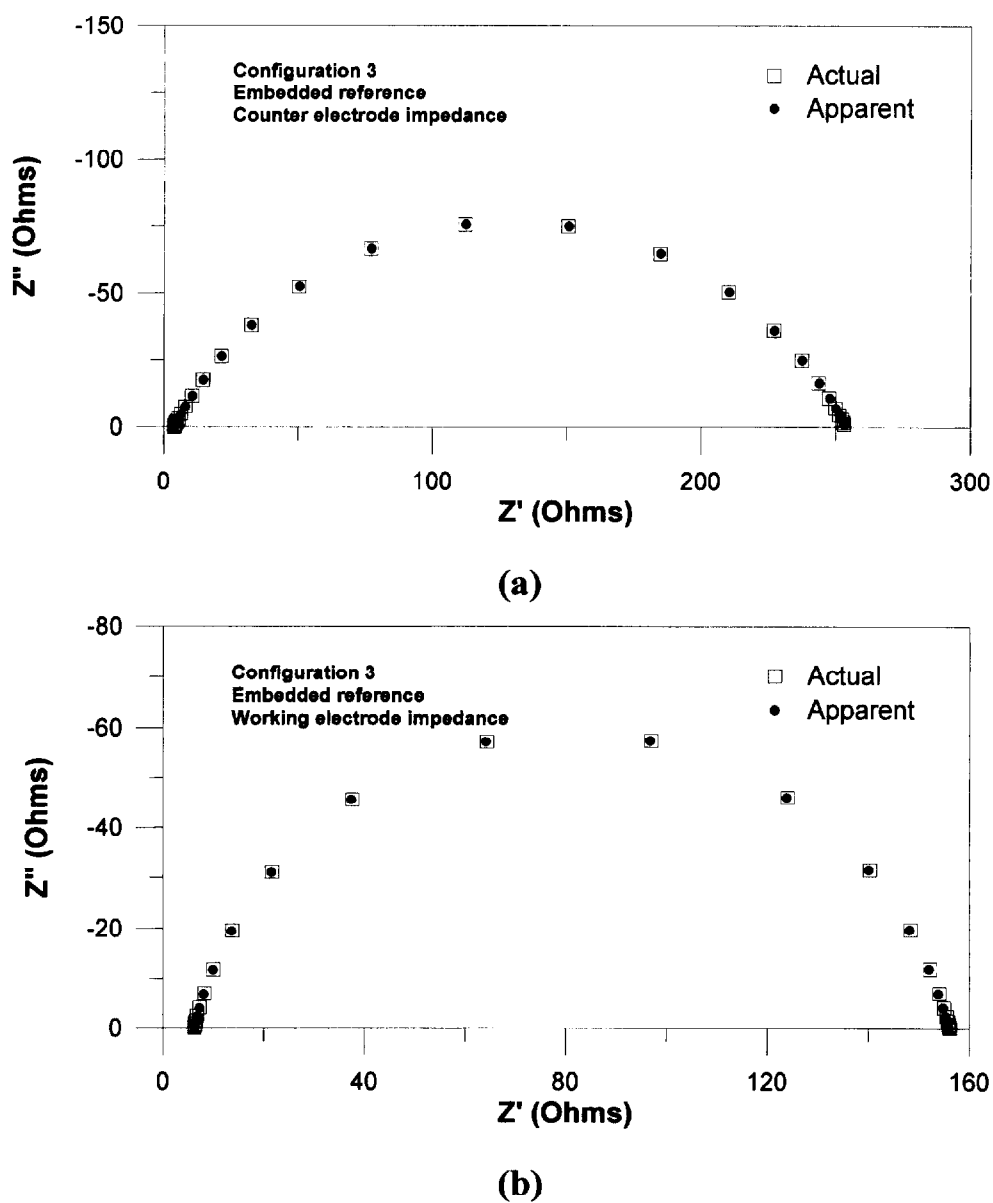


Fig. 5. Simulated actual ( $\square$ ) and apparent ( $\bullet$ ) impedance spectra using electrode configuration 3, the embedded reference electrode: (a) counter electrode; (b) working electrode.

surprisingly, total electrolyte resistance depends non-linearly on inverse aspect ratio, as shown in Fig. 7b. Presumably, at very large thicknesses, the relationship may approach linearity. The partitioning of the electrolyte resistance is also strongly dependent on aspect ratio (see Fig. 7c). At large  $d/t$  (small  $(d/t)^{-1}$ )

the effective potential surface sampled by the pseudoreference is very close to the working electrode, i.e.,  $R_{\text{offset}}(\text{WE}) \sim 0$ . With decreasing  $d/t$  (increasing thickness) the effective potential surface again moves toward the counter electrode. Because the apparent impedance spectra exhibit such gross distortions, one

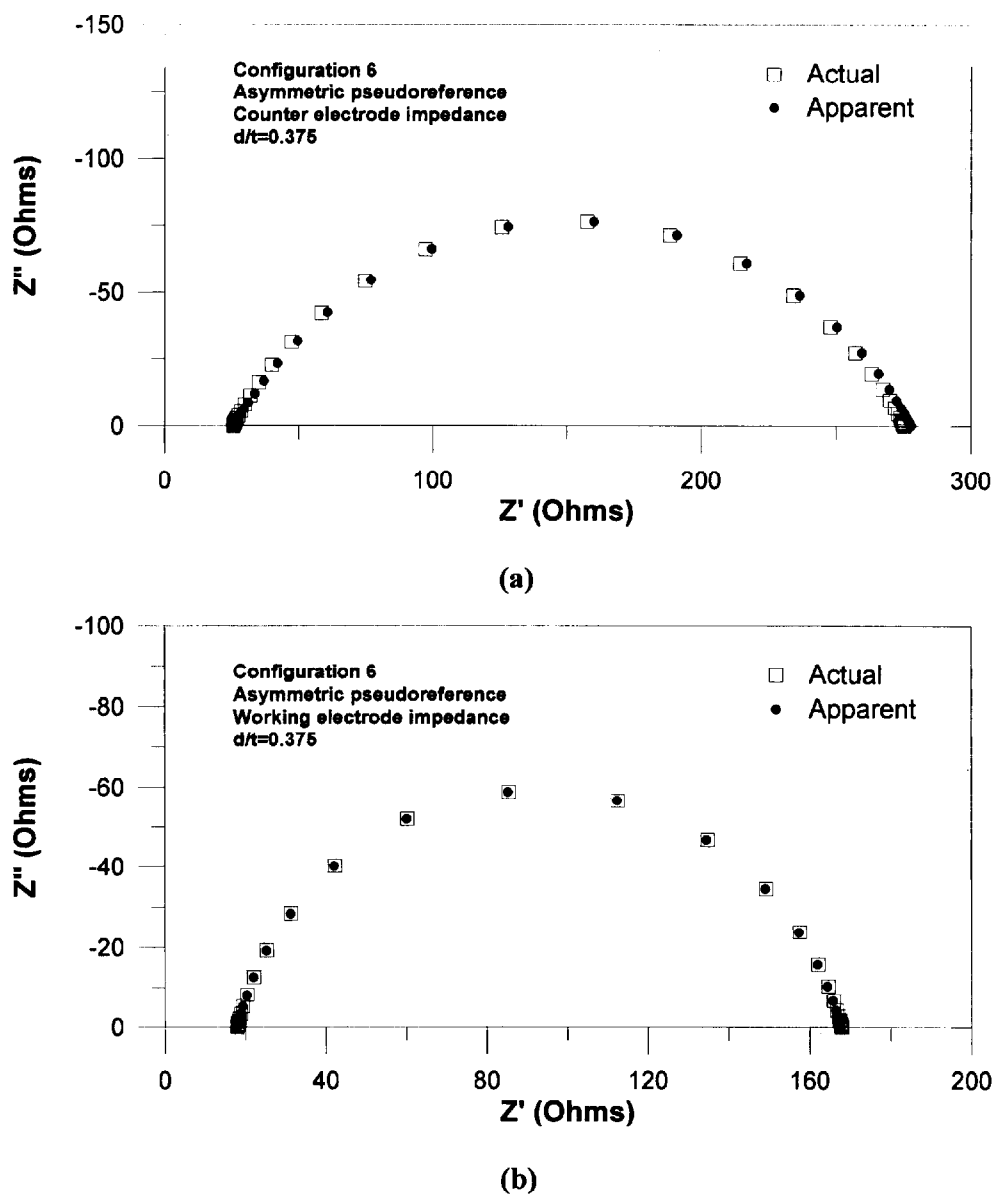
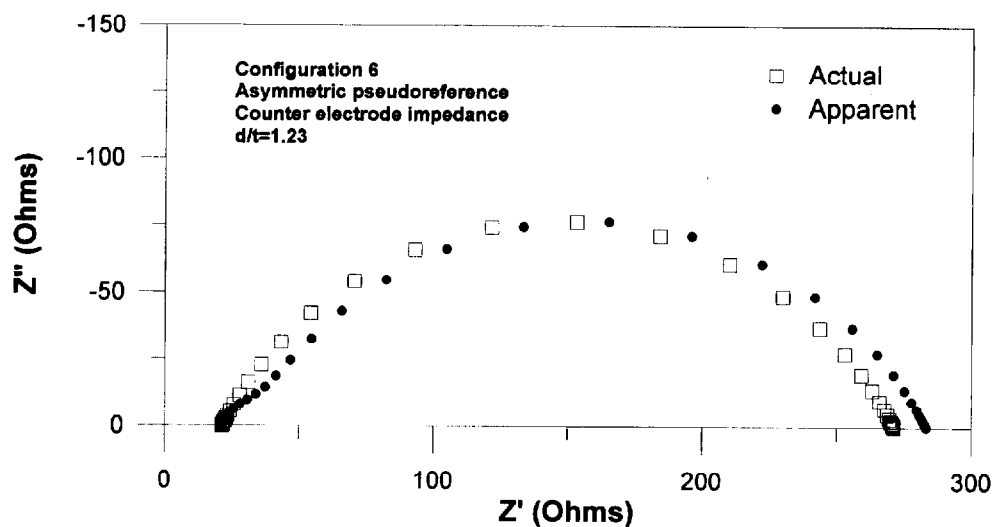


Fig. 6. Simulated actual (□) and apparent (●) impedance spectra using electrode configuration 6, the asymmetric pseudoreference electrode: (a) counter electrode,  $d/l = 0.375$ ; (b) working electrode,  $d/l = 0.375$ ; (c) counter electrode,  $d/l = 1.23$ ; (d) working electrode,  $d/l = 1.23$ ; (e) counter electrode,  $d/l = 2.46$ ; (f) working electrode,  $d/l = 2.46$ .

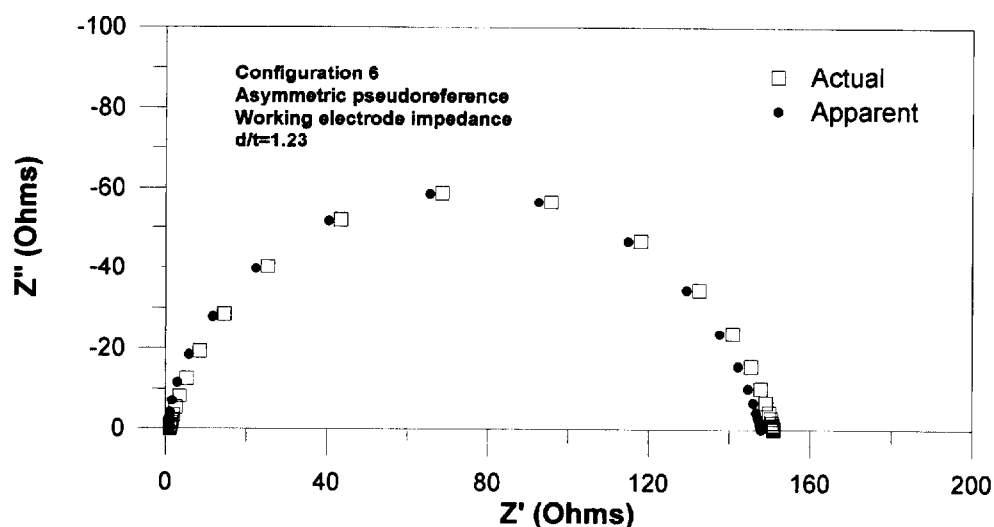
should exercise extreme care in employing such an asymmetric electrode configuration to make certain the measurement is in fact accurate.

When making measurements on a real electrode, the 'actual' response is unknown. To overcome this limitation, the dual-reference electrode cells of Fig. 2

were used. These cells allowed identical platinum electrodes to be characterized by both an embedded Luggin probe reference and an external pseudoreference. Based on the numerical simulations, measurements with the embedded RE are expected to be accurate. Furthermore, we have previously demon-



(c)

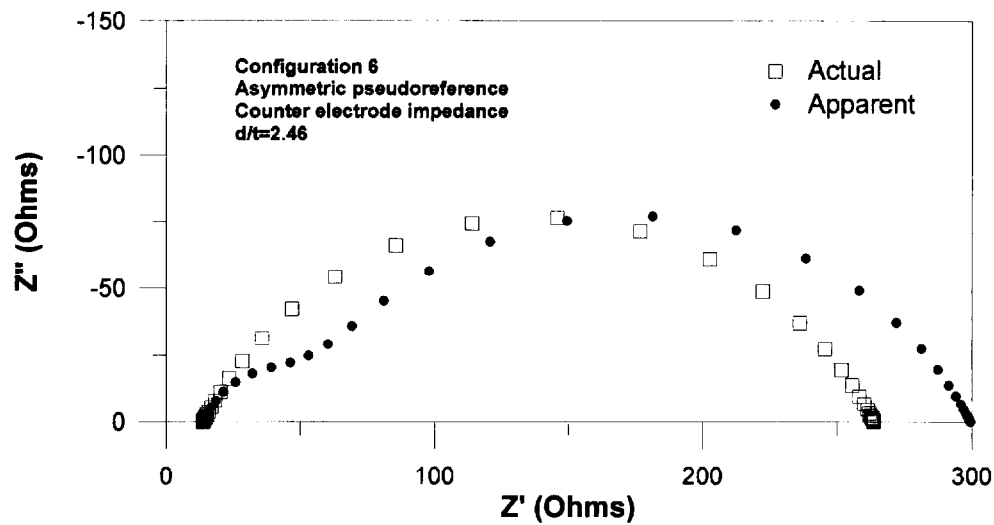


(d)

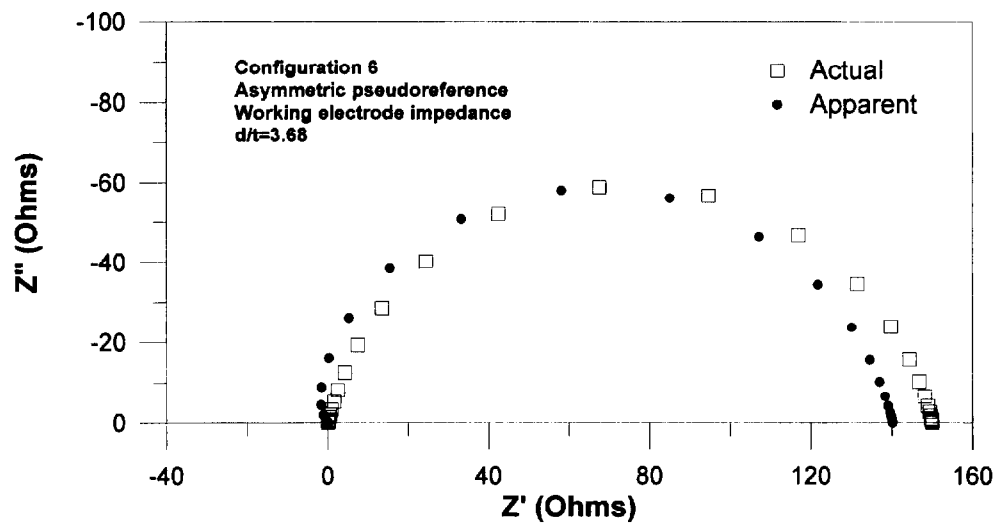
Fig. 6. (continued)

strated that silver dramatically reduces the reference electrode impedance and can be used in place of platinum to minimize voltage divider distortions [2]. The embedded silver RE spectrum is therefore used in place of an 'actual' spectrum, which is unavailable. The 'total cell impedances' in Figs. 8–10 were obtained by two-point method between the counter

and the working electrodes in order to find the overall electrolyte resistances. These total spectra appear only in the high frequency insets. The impedance spectra in Fig. 8, measured using the platinum pseudoreference in configuration 1 (see Fig. 2a), are very similar to that obtained from the embedded silver RE. The only difference is a slight systematic



(e)



(f)

Fig. 6. (continued)

shift in the  $Z'$  axis. From the computer simulations, it was expected that configuration 1 can measure electrode responses fairly accurately. Although the aspect ratio  $d/t$  is not large, there is still no noticeable distortion. The shift along the  $Z'$  axis is the result of different effective potentials at the RE, as described previously, and corresponds to the peculiar

partitioning of the electrolyte resistance (see the high frequency inset diagrams). The partitioning in the case of the embedded silver RE is 25%/75%, in agreement with the geometric construction of the cell. For the external platinum pseudoreference, the partitioning is 70%/30%. Deviation from 50%/50% (see Table 2, configuration 1 and Fig. 4c) arises from

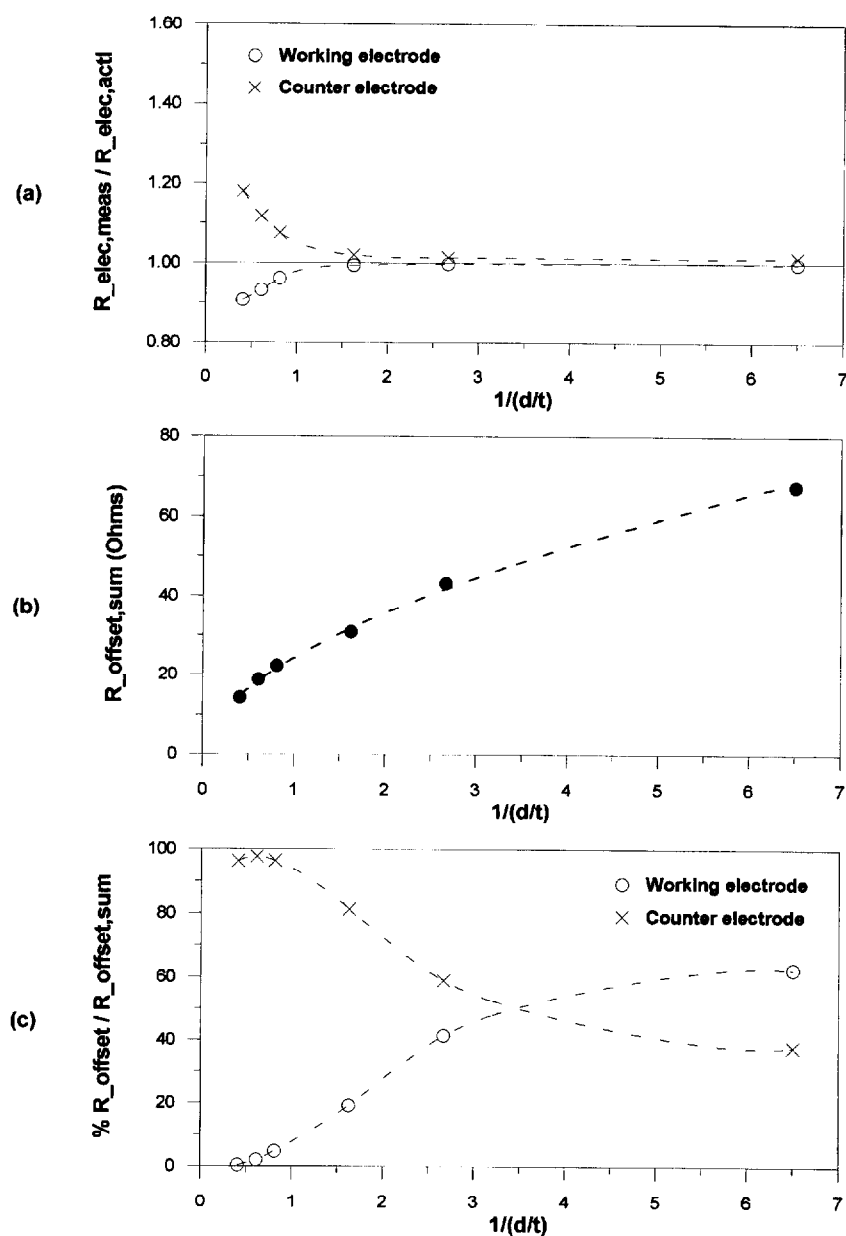


Fig. 7. Effect of aspect ratio  $d/t$  on the accuracy of asymmetric electrode configuration 6: (a) deviation of apparent magnitude of working electrode (O) and counter electrode (X) arc from input parameters; (b) total electrolyte resistance; (c) individual partitioning of electrolyte.

insufficiently large  $d/t$ . Thus, although the aspect ratio does not satisfy the condition to evenly split the electrolyte resistance, the remainder of each impedance spectrum is nonetheless correct.

Measurements obtained from the cells in Fig. 2b

are plotted in Figs. 9 and 10. Two aspect ratios were examined:  $d/t = 0.35$  in Fig. 9 and  $d/t = 1.82$  in Fig. 10. For  $d/t = 0.35$ , results are similar to those in Fig. 8 in that the electrode arcs are simply displaced along the  $Z'$  axis. From Fig. 7a, no significant

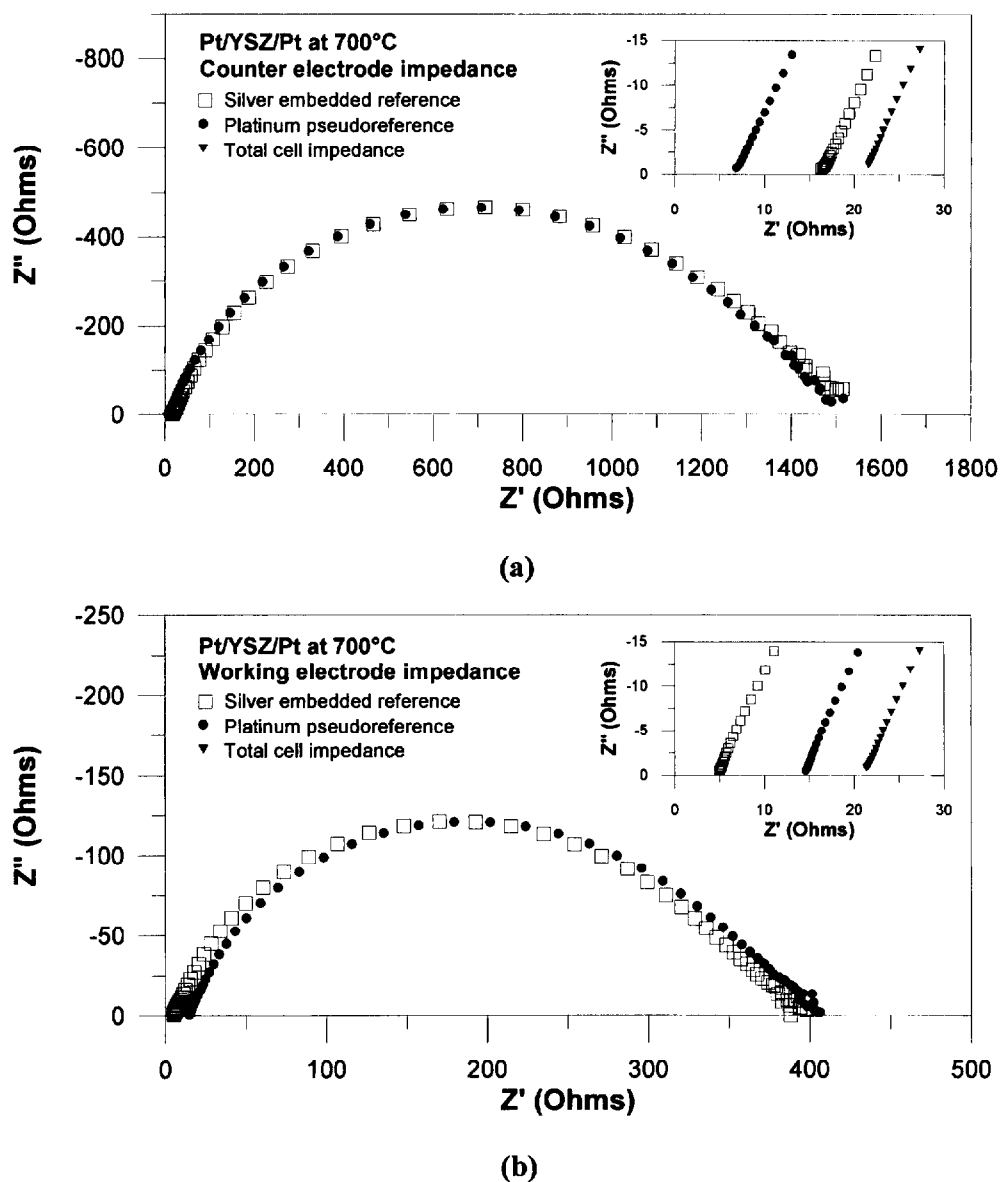


Fig. 8. Impedance spectra measured by a platinum pseudoreference (●) in configuration 1 at  $d/t = 0.14$  and an embedded silver reference (□) in configuration 3: (a) counter electrode impedance; (b) working electrode impedance. Inset shows high frequency portion with total cell impedance (▼).

distortion was expected at this aspect ratio. Furthermore, the partition of the electrolyte resistance is in agreement with simulation. On increasing the aspect ratio to 1.82, however, a different picture emerges. In Fig. 10b, the working electrode spectrum is clearly distorted, with a prominent phase shift toward larger

phase angles at high frequencies, similar to the lopsided spectra shown in Fig. 6d and Fig. 6f. Furthermore, in addition to a shift in  $Z'$ , the size of the WE arc is incorrect. Curiously, however, the counter electrode spectrum does not exhibit any spurious high frequency arcs. This may be explained

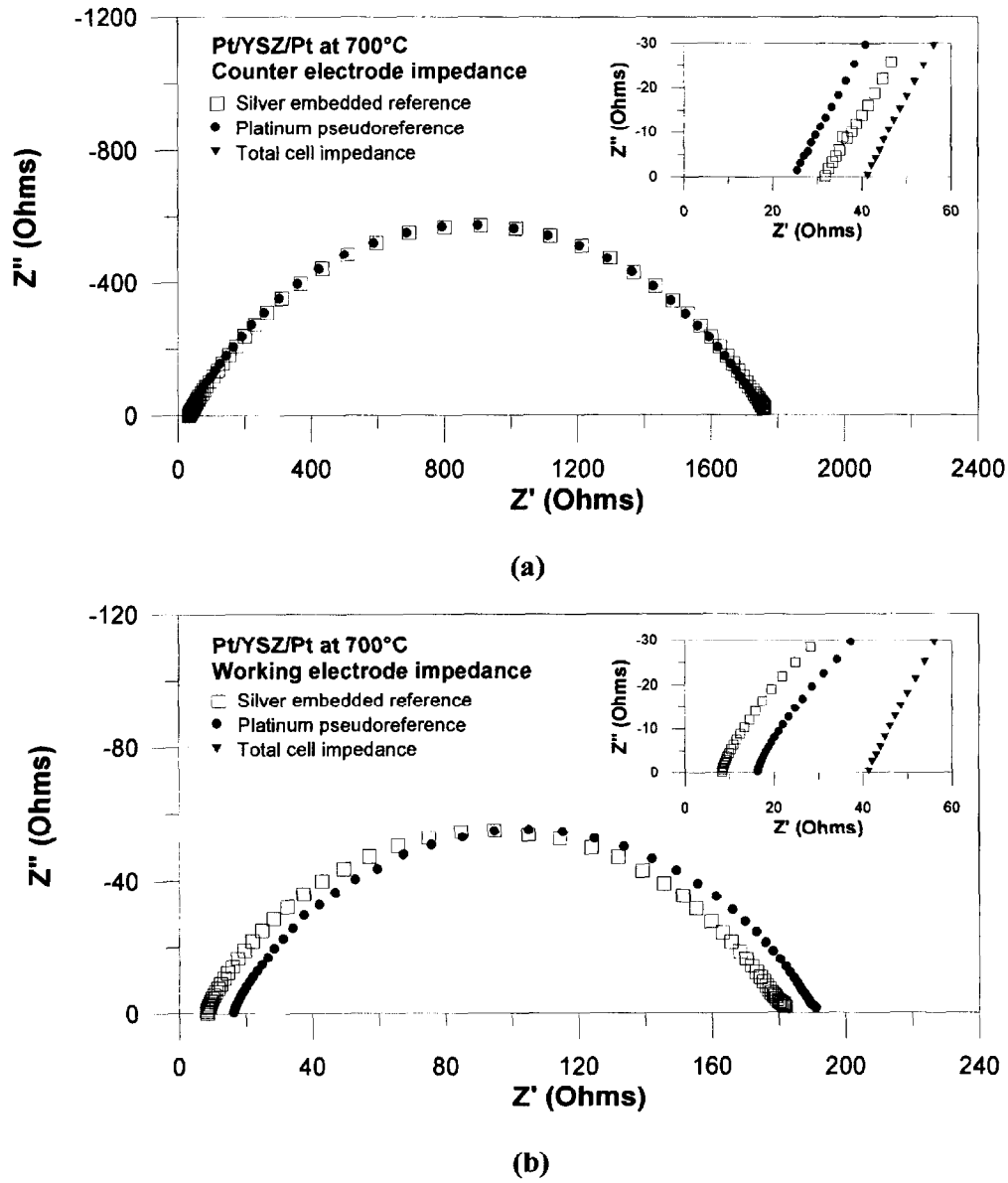


Fig. 9. Impedance spectra measured by a platinum pseudoreference (●) in configuration 6 at  $d/t = 0.35$  and an embedded silver reference (□) in configuration 3: (a) counter electrode impedance; (b) working electrode impedance. Inset shows high frequency portion with total cell impedance (▼).

by the fact that the counter electrode impedance is much, much larger than the working electrode impedance, partially due to differences in electrode preparation and partially due to differences in electrode areas. A distortion that is significantly large in

relation to the working electrode impedance is negligible when superimposed on the counter electrode impedance. Note, however, the nearly 0%/100% split in the electrolyte resistance, which is in agreement with Fig. 7c. To confirm that one can

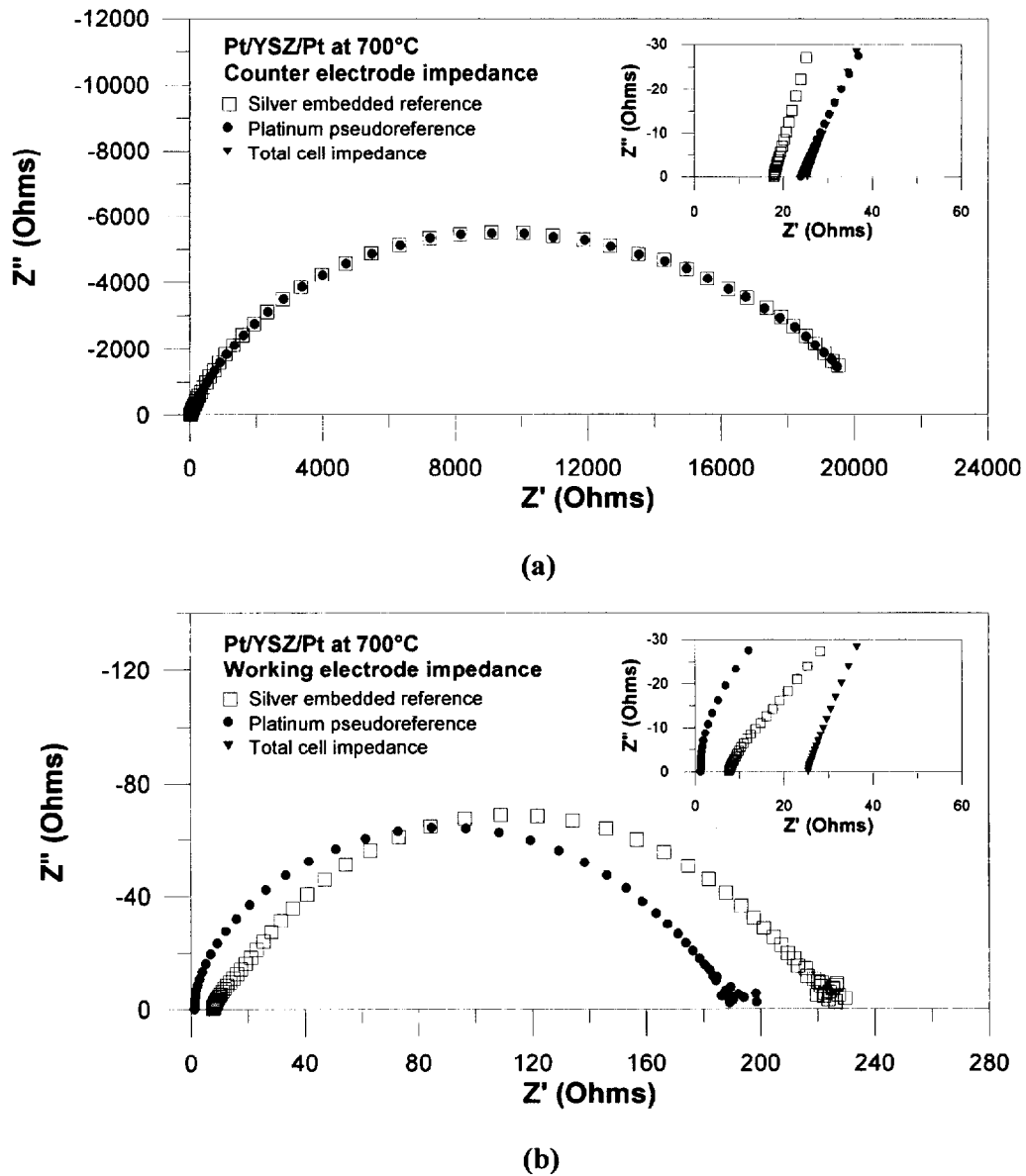


Fig. 10. Impedance spectra measured by a platinum pseudoreference (●) in configuration 6 at  $d/l = 1.82$  and an embedded silver reference (□) in configuration 3: (a) counter electrode impedance; (b) working electrode impedance. Inset shows high frequency portion with total cell impedance (▼).

observe distorted WE spectra without a distorted CE spectrum, another set of simulations was performed, with input parameters for the simulation obtained from complex non-linear least squares fitting of the embedded silver WE and CE spectra. Results are

shown in Fig. 11. The working electrode spectra exhibited a distorted, lopsided arc, although not as pronounced as that observed in Fig. 10b. Just as in the actual experiment, the counter electrode spectrum does not show any significant distortion.

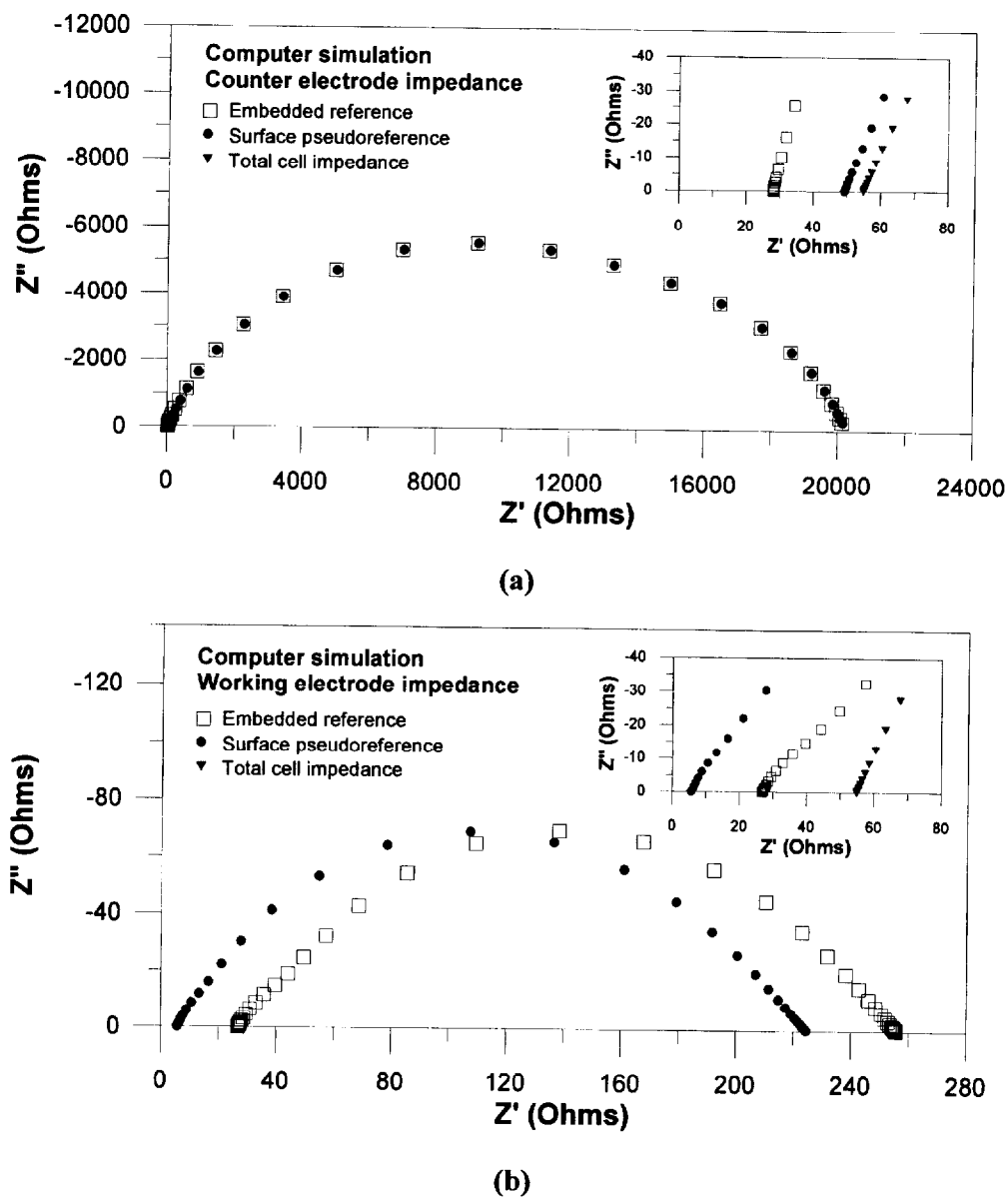


Fig. 11. Simulated impedance spectra measured by a pseudoreference (●) in configuration 6 at  $d/t = 1.82$  and an embedded reference (□) in configuration 3: (a) counter electrode impedance; (b) working electrode impedance. Inset shows high frequency portion with total cell impedance (▼).

#### 4. Conclusions

Experiments and computer simulations confirmed that the accuracy of three-point impedance measurements depends on the geometry and placement of the reference electrode. For configurations where the

pseudoreference electrode is not located at infinity with respect to the counter and the working electrode, nonuniform current density causes 'area' (instead of 'point') reference electrodes to sample many equipotential surfaces. The averaged potential changes with electrode configuration. Electrolyte

resistance partitioning gives an indication of the location of the effective equipotential surface within the electrolyte. There is no simple relationship between electrolyte resistance and the geometry of the cell when surface mounted pseudoreference electrodes are involved. In contrast, the equipotential surface sampled by the Luggin probe-type reference electrode is well defined, and the electrolyte resistance scales linearly with electrode separation.

Electrode impedances are affected by reference electrode geometry/position as well. An embedded reference electrode accurately measures both counter and working electrode impedances as long as electrode spacing is significantly larger than the radius of the probe, and the presence of the reference electrode does not significantly perturb the primary current (i.e., the Luggin probe hole must be small compared to the diameter of the sample). When using pseudoreference electrodes, caution is necessary as measurements may be inaccurate. Experiments and simulations show that for a symmetric electrode geometry (e.g. configuration 1 of Fig. 1), the pseudoreference can be treated as if it is located within the electrode midway between the counter and working electrodes when the aspect ratio is comparable or larger than unity (thin samples). There is no appreciable error in electrode impedance. At smaller aspect ratios, the electrolyte resistance partitions unevenly, and error in electrode impedance gradually increases to 1% ~ 2% at  $d/t = 0.20$ . No spurious arcs were observed. With an asymmetric electrode geometry (e.g. configuration 6 of Fig. 1), the ill-defined nature of the reference potential can introduce significant distortions. For large aspect ratios (thin samples), the partitioning of electrolyte resistance is nearly 0%/100% (RE/WE)/(RE/CE), and the electrode impedance is in error by 10% ~ 20%. Furthermore, the impedance spectra exhibit phase shifts and spurious arcs. Spectra are highly unreliable at large aspect ratios (thin samples). On decreasing  $d/t$  (thicker samples) the quality of the data improves. Below  $d/t = 0.50$ , the error is reduced to only a few percent. Unlike the symmetric configuration, however, electrolyte partitioning does not appear to approach some fixed value.

Although it is slightly more complicated experimentally, the safest approach for accurate solid electrolyte/electrode studies is to use a Luggin

probe-type reference electrode. Since a point contact is employed, care must be taken to minimize the impedance of the reference electrode so that it remains small relative to the input impedance of the impedance analyzer [2]. If an external pseudoreference electrode must be used, it is important to establish whether or not reliable electrode measurements can be made and over what range of aspect ratios. This is best done by computer simulation or, alternatively, in preliminary tests using a dual-reference (external, internal) cell as in Fig. 2.

### Acknowledgments

This work was supported by the U.S. Department of Energy/Fossil Energy AR and TD Materials Program (GH, LRP) and the National Science Foundation Materials Research Science and Engineering Centers Program under grant no. DMR-91-20521 (TOM). George Hsieh acknowledges the support of a National Defense Science and Engineering Graduate Fellowship.

### References

- [1] G. Hsieh, S.J. Ford, T.O. Mason and L.R. Pederson, *Solid State Ionics* 91 (1996) 191.
- [2] G. Hsieh, T.O. Mason and L.R. Pederson, *Solid State Ionics* 91 (1996) 203.
- [3] C. Kasper, *Trans. Electrochem. Soc.* 77 (1940) 353.
- [4] S. Barnartt, *J. Electrochem. Soc.* 98 (1951) 311.
- [5] S. Pizzini, M. Bianchi, A. Corradi and C. Mari, *J. Appl. Electrochem.* 4 (1974) 7.
- [6] W.H. Tiedemann, J. Newman and D.N. Bennion, *J. Electrochem. Soc.* 120 (1973) 256.
- [7] A.C. West and J. Newman, *J. Electrochem. Soc.* 136 (1989) 139.
- [8] M. Nagata, Y. Itoh and H. Iwahara, *Solid State Ionics* 67 (1994) 215.
- [9] F.H. van Heuveln, F.P.F. van Berkel and J.P.P. Huijsmans, *Proceedings of the 14th Risø International Symposium on Materials Science*, eds. F.W. Poulsen, J.J. Bentzen, T. Jacobsen, E. Skou and M.J.L. Østergård (1993) 53.
- [10] S. Barnartt, *J. Electrochem. Soc.* 99 (1952) 549.
- [11] J. Newman and W. Tiedemann, *J. Electrochem. Soc.* 140 (1993) 1961.
- [12] C. Fiaud, M. Keddad, A. Kadri and H. Takenouti, *Electrochimica Acta* 32 (1987) 445.
- [13] B. Gharbage, T. Pagnier and A. Hammou, *J. Electrochem. Soc.* 141 (1994) 2118.

- [14] T. Kawada, N. Sakai, H. Tokokawa, M. Dokiya, M. Mori and T. Iwata, *J. Electrochem. Soc.* 137 (1990) 3042.
- [15] J. Mizusaki, H. Tagawa, K. Tsuneyoshi and A. Sawata, *J. Electrochem. Soc.* 128 (1991) 1867.
- [16] A.J.A. Winnubst, A.H.A. Scharenborg and A.J. Burggraaf, *Solid State Ionics* 14 (1984) 319.
- [17] E.J.L. Schouler and M. Kleitz, *J. Electrochem. Soc.* 134 (1987) 1045.
- [18] J. Mizusaki, K. Amano, S. Yamauchi and K. Fueki, *Solid State Ionics* 22 (1987) 313.
- [19] S.P.S. Badwal and H.J. de Bruin, *J. Electrochem. Soc.* 129 (1982) 1921.
- [20] G.E. Youngblood, C.F. Windisch and J.L. Bates, *Proceedings of the 14th Risø International Symposium on Materials Science*, eds. F.W. Poulsen, J.J. Bentzen, T. Jacobsen, E. Skou and M.J.L. Østergård (1993) 479.
- [21] M.J.L. Østergård and M. Mogensen, *Electrochimica Acta* 38 (1993) 2015.
- [22] D.M. Reed, H.U. Anderson and W. Huebner, *J. Electrochem. Soc.* 143 (1996) 1558.
- [23] B.A. Boukamp, EQUIVCRT program V3.97 (1989).
- [24] R.T. Coverdale, E.J. Garboczi, H.M. Jennings, B.J. Christensen and T.O. Mason, *J. Am. Ceram. Soc.* 76 (1993) 1513.
- [25] R.T. Coverdale, B.J. Christensen, T.O. Mason, H.M. Jennings and E.J. Garboczi, *J. Mater. Sci.* 29 (1994) 4984.
- [26] R.T. Coverdale, B.J. Christensen, T.O. Mason, H.M. Jennings, D.P. Bentz and E.J. Garboczi, *J. Mater. Sci.* 30 (1995) 712.
- [27] R.T. Coverdale, H.M. Jennings and E.J. Garboczi, *Comp. Mater. Sci.* 3 (1995) 465.
- [28] R.D. Cook, D.S. Malkus and M.E. Plesha, *Concepts and Applications of Finite Element Analysis* (Wiley, New York, 1989).
- [29] W.H. Press, B.P. Flannery, S.A. Teukolsky and W.T. Vetterling, *Numerical Recipes: The Art of Scientific Computation (FORTRAN)* (Cambridge Univ. Press, Cambridge, 1989).